ACS APPLIED MATERIALS & INTERFACES

Surfaces, Interfaces, and Applications

Eu luminescence in high charge mica: an in situ probe for the encapsulation of radioactive waste in geological repositories

Rosa Martín-Rodríguez, Fernando Aguado, Maria Dolores Alba, Rafael Valiente, and Ana Carmen Perdigón

ACS Appl. Mater. Interfaces, **Just Accepted Manuscript** • DOI: 10.1021/acsami.8b20030 • Publication Date (Web): 23 Jan 2019

Just Accepted

ACS Publications

is published by the American Chemical Society. 1155 Sixteenth Street N.W., Washington, DC 20036

Eu^{3+} luminescence in high charge mica: an *in situ* probe for the encapsulation of radioactive waste in geological repositories

Rosa Martín-Rodríguez[†,‡], Fernando Aguado[‡,§], María D. Alba[&], Rafael Valiente[‡,ψ] and Ana C. Perdigón[†,‡]*

[†]QUIPRE Department, University of Cantabria, Avda. de Los Castros 46, 39005 Santander, Spain. [‡]Nanomedicine Group, IDIVAL, Avda. Cardenal Herrera Oria s/n, 39011 Santander, Spain. [§]CITIMAC Department, University of Cantabria, Avda. de Los Castros 48, 39005 Santander, Spain. [&]Instituto Ciencia de los Materiales de Sevilla, CSIC-US, Américo Vespucio 49, 41092 Sevilla, Spain.[ψ] Applied Physics Department, University of Cantabria, Avda. de Los Castros 48, 39005 Santander, Spain.

KEYWORDS: high charge micas, surface interaction, europium luminescence, radioactive waste, europium disilicate

ABSTRACT. Isolation of high-level radioactive waste (HLW) in deep geological repositories (DGR) through a multi-barrier concept is the most accepted approach to ensure long-term safety. Clay minerals are one of the most promising materials to be used as engineered barriers. In particular, high charge micas, as components of the engineered barrier, show super-selectivity for some radioactive isotopes and a large adsorption capacity, which is almost twice as the other low charge aluminosilicates. In addition, high charge micas are optimum candidates for decontamination of nuclear waste through two different mechanisms; namely an ion exchange reaction and a non-reversible mechanism involving the formation of new stable crystalline phases under hydrothermal conditions. In this paper we report a new *in situ* optical sensor based on the incorporation of Eu^{3+} in these high charge micas for tracking the long-term physical-chemical behaviour of HLW contaminants in DRG under mild hydrothermal conditions. The incorporation of Eu^{3+} into the interlayer space of the mica originates a well resolved green and red luminescence, from both the $^5D_1$ and $^5D_0$ excited states, respectively. The formation of new crystalline phases under hydrothermal conditions involves important changes in the Eu^{3+} emission spectra and lifetime. The most interesting features of Eu^{3+} luminescence to be used as an optical sensor are: (1) the presence or absence of the Eu^{3+} green emission from the $^5D_1$ excited state, (2) the energy shift of the $^5D_0 \rightarrow {}^7F_0$ transition, (3) the crystal-field splitting of the $^7F_1$ Eu^{3+} level, and (4) the observed luminescence lifetimes, which are directly related to the interaction mechanisms between the lanthanide ions and the silicate network.

1. INTRODUCTION

High-level radioactive waste (HLW) requires a great level of isolation from the environment to assure long-term storage. It contains both short- and long-lived radionuclides having as differentiating feature the generation of significant quantities of heat from radioactive decay, which is expected to be extended for centuries.[1] Isolation of the HLW in deep geological repositories (DGR), through a multi-barrier concept, is currently the most accepted approach adopted by Governments to ensure long-term safety, considering that storage periods range from 500 to 10^6 years.[2] DGR consist of a series of engineered and natural barriers linked, with the purpose of retarding or retaining the radionuclides in the event of a possible leak to the biosphere. In the nuclear waste retention strategy, bentonites, swelling clays composed by an 85% of montmorillonite, have been chosen as part of the engineered barrier system (EBS) as the ideal backfill material in DGR to be used around containers, to seal the tunnel and boreholes.[3,4] The family of synthetic highly charged sodium fluorophlogopite micas, called high charge micas, of composition $Na_xAl_xSi_{(8-x)}Mg_6O_{20}F_4$, x =2 and 4, firstly synthesized by Gregorkiewitz et al., have been previously probed to be excellent candidates as alternative clay mineral for the EBS.[5] Despite the large negative charge in its layered structure, high charge micas, unlike natural brittle micas, exhibit a high cation exchange capacity and an unexpected thermal stability.[6] Its adsorption capacity is on the same order of Al-rich zeolites, with theoretical cation exchange values up to four times higher than other low charged aluminosilicates.[7]

The capture and subsequent immobilization of radionuclides in the structure of swelling clay minerals involve mainly two different chemical mechanisms: Firstly, a sorption reaction in the aqueous solution interface of the clay by cation exchange reaction or, alternatively, a chemical interaction of the actinide ions with the surface and edges of the clay, at ambient temperature.

Secondly, a less explored mechanism based on a chemical reaction between the actinides and the clay minerals under mild hydrothermal conditions, where the interlayer cations and the silicon atoms react to form new disilicate crystalline phases.[8,9] The processes undertaken at room temperature are highly dependent on the physical-chemical properties of the cation such as, hydration energy and electrostatic parameter. Besides, different structural parameters of the clay, like type of mineral, surface functional groups, as well as value and origin of the layer charge also play a fundamental role in the actinide-clay interaction nature.[10] Thus, under this chemical route, the capture of the radioactive cations is generally a reversible process where any variation of the conditions of the clay aqueous solution, mainly pH or ionic strength, affects the sorption equilibrium. As a consequence, the radioactive waste can be released back to the geosphere from the EBS.

High charge micas represent a highly versatile candidate to be used as sealing material through the second aforementioned mechanism; a chemical reaction under hydrothermal conditions. In particular, a super-selectivity and stable immobilization has been previously described by Komarneni *et al.* for the ^{137}Cs and ^{226}Ra, radioactive isotopes through electrostatic bonding at room temperature.[11,12] An incomplete cation exchange reaction was described, followed by the collapse of the interlayer spacing of the clay. For the study of the less-explored second mechanism, in other clays where the silicate network interacts with the interlayer cation under hydrothermal conditions, lanthanides cations have been used as actinide simulators.[8] The thermal stability of clay is a crucial parameter concerning the long-term behavior of the DGR. Considering the rate at which groundwater diffuses to the fill material, hydrothermal conditions may be expected in the borehole. In that scenario, a peak temperature of approximately 200°C is predicted in the packing material shortly after repository close, with temperatures above 150°C

for the next 500 years.[13,14] However, to evaluate the reaction process between the argillaceous material and the lanthanides, as actinide simulators, most of previous studies have been carried out at temperatures up to 350°C to increases the reaction kinetic.[15] Regarding the second retention mechanism, key structural parameters that enhance the reactivity of clays with cations in aqueous solution and formation of new crystalline phases under mild hydrothermal conditions have been previously identified: (1) Full occupancy of the octahedral structural sites by lithium or magnesium, since the incorporation of rare-earth cations from the interlayer space in the new disilicate/ortosilicate phases requires the migration of octahedral cations to these positions. (2) High content of the isomorphic substitutions of aluminum cations by silicon in the tetrahedral sheet of the silicate. The more localized negative charge in the vicinity of the silicon atom due to the proximity of tetrahedral aluminum, the higher electrostatic interaction between these ions and the interlayer rare-earth cations.[16] High charge micas are trioctahedral clays with a Si:Al ratio in the tetrahedral sheet from 3:1 to 1:1. This particular structural feature makes this family of synthetic clays an optimum candidate for decontamination of nuclear waste not only through an ion exchange reaction but mainly through the formation of new crystalline phases.[9]

Luminescent lanthanide ions have been previously used as models to study the surface interaction and retention processes of trivalent actinides. In particular, the emission of Eu^{3+} has been used as a probe to investigate their adsorption and complexation mechanism in a variety of low charge aluminosilicates, such as montmorillonite and saponite, as a function of pH and at different temperatures.[17,18] Interestingly, active radionuclides ^{153}Eu, ^{154}Eu and ^{155}Eu are components of the spent nuclear fuel.[19] However, in previous works, only broad and non-well resolved Eu^{3+} luminescence bands, due to transitions from the $^5D_0$ excited state were observed, mainly caused by the low crystallinity of clays because of its natural origin.[20] Recently, we have

reported highly efficient photoluminescence from isolated Eu^{3+} incorporated in a high charge mica.[21] Eu^{3+} cations are allocated in the interlayer space of the aluminosilicate as inner-sphere complexes, coordinated with 2.9 water molecules in a first coordination sphere completed with the structural basal oxygens of the clay surface.[21] This clay fulfils the requirements to be used as a luminescent sensor in the following terms: (1) High charge micas are synthetic clays, therefore, undesirable impurities such as iron, responsible for luminescence quenching, are not present. (2) High charge micas are fluorinated clays with non-hydroxyl groups in its structure, which also cause luminescence deactivation through non-radiative processes. (3) The presence of Al^{3+} in the tetrahedral sheet acts as an intrinsic dispersing agent, avoiding the clustering of lanthanide ions and enhancing Eu^{3+} luminescence.[22]

Here, we present a new *in situ* optical sensor based on the incorporation of Eu^{3+} in a high charge mica with 2 negative charges per unit cell, hereafter Mica-2, for tracking the long-term physical-chemical behaviour of HLW contaminants in DGR under mild hydrothermal conditions. Contrary to other techniques, such as X-ray diffraction, which requires sample preparation and measurement in *ex situ* equipment, spectroscopic measurements can be performed *in situ* by using a fiber for excitation and detection. As mentioned before, sharp-line Eu^{3+} emission is an ideal candidate to be used as spectroscopic probe, since both, the fine structure and the relative intensity of different transitions as well as the luminescence lifetime can be used to characterize the local environment of Eu^{3+} ions. Although some europium isotopes are already part of the radioactive waste, considering its low amount, addition of a Eu^{3+} salt to the canister might be desirable. Thus, Eu^{3+} sharp-line luminescence provides valuable information concerning the crystalline structure of the host material.

2. EXPERIMENTAL SECTION

2.1 Synthesis of Mica-2

Near-stoichiometric powder mixtures with the molar composition 6 SiO_2, 1 $Al(OH)_3$, 6 MgF_2, and 2 NaCl were used to synthesize the Mica-2 starting sample. The starting materials were SiO_2 from Sigma (CAS No. 112945-52-5 99.8% puriry), $Al(OH)_3$ from Riedel-de Haën (CAS No. 21645-51-2, 99% purity), MgF_2 from Aldrich (CAS No. 20831-0, 98% purity), and NaCl from Panreac (CAS No. 131659, 99.5% purity). All reagents were mixed and ground before heating up to 900 °C in a Pt crucible for 15 h. After cooling, the solids were washed with deionized water and dried at room temperature.

2.2 Cation exchange reaction

Mica-2 was subjected to an aqueous ion exchange with Eu^{3+} as follows: 300 mg of clay were dispersed in 50 ml of deionized water solution of $Eu(NO_3)_3$ (REacton 99.99%) with a five-fold cation exchange capacity concentration (247 meq/100 g) for 48 h. This process was repeated three more times. Samples were washed and centrifuged with deionized water.

2.3 Hydrothermal treatments

300 mg of the powdered Mica-2 were dispersed in 50 ml of $5 \cdot 10^{-2}$ M $Eu(NO_3)_3$ solutions and were heated in a stainless steel reactor, at different temperatures (150, 200 and 300°C) and diverse times (0, 2, 15 and 30 days). The reaction products were collected by filtering using a Millipore filter with 0.45 μm pore diameter, washed with distilled water, and dried in air at 60 °C.

2.4 Optical characterization

Steady state luminescence, excitation and lifetime measurements were performed using a FLSP920 spectrofluorometer (Edinburgh Instruments) equipped with double-monochromators, a continuous Xe-lamp of 450 W and a pulsed Xe-lamp of 60 W (μF920) for excitation, and a Hamamatsu R928 photomultiplier tube (PMT) for detection. All emission spectra were corrected for the system response. The excitation and emission spectra were normalized to the intensity of the $^7F_0 \rightarrow {}^5L_6$ and $^5D_0 \rightarrow {}^7F_2$ transitions, respectively, and an offset was applied for the sake of clarity.

3. RESULTS AND DISCUSSION

3.1 Generation of new crystalline phases from Mica-2 under hydrothermal treatments

The effect of temperature and time on the retention of Eu^{3+} by Mica-2 has been previously analyzed in detail by X-ray diffraction and presented elsewhere.[23] The major conclusions of the study are introduced below. Figure 1a displays a representation of the predominant crystalline phases obtained after hydrothermal treatment of the high charge Mica-2 with a $Eu(NO_3)_3$ solution in a stainless steel reactor as function of temperature and time under subcritical conditions, similar to long-term conditions of the DGRs. The energy level scheme of Eu^{3+} ions, with the transitions responsible for red and green luminescence, is presented in Figure 1b.

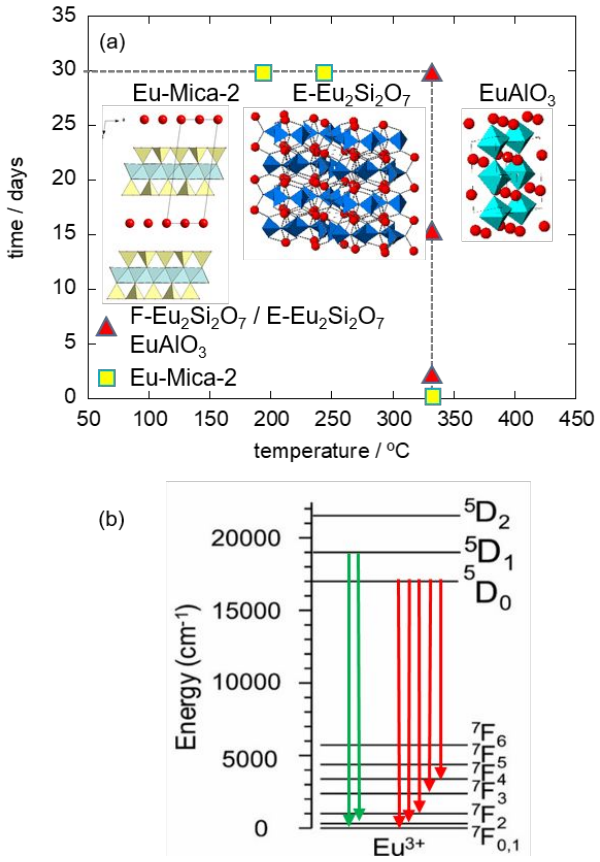

Figure 1. (a) Representation of Mica-2 phase and the predominant crystalline structures obtained after hydrothermal treatment as function of temperature and time, as deduced from X-ray diffraction in ref. 24. (b) Eu^{3+} energy level diagram showing the transitions responsible for red and green Eu^{3+} luminescence, from the $^5D_0$ and $^5D_1$ excited states, respectively.

Regarding temperature dependence, treatments at 150 and 200°C for a month cause the incorporation of hydrated Eu^{3+} cations to the interlayer space of the aluminosilicate along with some disruption of the silicate network. At those temperatures, ion exchange reaction is the primary mechanism for europium adsorption. X-ray diffraction measurements also showed new reflections that correspond to the incipient crystallization of secondary phases resulting from the mica disruption and from the interaction of Eu^{3+} with the mica framework.[23] However, higher

temperatures are needed to fully develop other crystalline phases containing Eu^{3+}, particularly, at 300°C, the system Mica-2/$Eu(NO_3)_3$ hydrothermally treated for a month forms other silicate phases, mainly disilicates (F-$Eu_2Si_2O_7$ and E-$Eu_2Si_2O_7$) and in a lower proportion aluminates ($EuAlO_3$). $Eu_2Si_2O_7$ is a pyrosilicate containing $(Si_2O_7)^{6-}$ structural units, where two silicon tetrahedral share one corner. $EuAlO_3$ is an aluminate that belongs to the families of ABO_3 perovskites oxides.

Considering different treatment times, it is worth noting that at 0 days and 300°C (these conditions imply a heated ramp up to 300°C of the system Mica-2/$Eu(NO_3)_3$ solution, followed by the cooling of the sample at room temperature), Eu^{3+} adsorption occurs in slightly higher amounts compared to the cation exchange capacity of Mica-2, confirming that Eu^{3+} cations are adsorbed in the bidimensional galleries of the high charge mica. On the contrary, after 2 days of treatment, other mechanisms such as specific chemical reaction between Eu^{3+} and the silicate matrix are involved, with formation of orto/disilicates and aluminates as secondary crystalline phases. These phases grow up after one week reaction and remain practically constant up to one month.

3.2 Optical properties of Eu^{3+} in Mica-2

Several efforts have been made to study the sorption mechanism of Eu^{3+} on other silicates, mainly montmorillonite as the principal component of bentonites,[24,25] through luminescence measurements, since both the intensity of the hypersensitive $^5D_0 \rightarrow {}^7F_2$ transition and the ratio of the $^5D_0 \rightarrow {}^7F_2$ and $^5D_0 \rightarrow {}^7F_1$ bands depend on the atomic environment of Eu^{3+}. However, emission spectra of adsorbed Eu^{3+} cations onto those silicates are weak and broader, due to variations in the second coordination sphere of Eu^{3+}, and univocal information cannot be

extrapolated from the optical experiments. On the contrary, luminescence of Eu^{3+} ions incorporated in the interlayer space of mica consists of sharp-line emission peaks due to transitions from both the $^5D_1$ and $^5D_0$ excited states to the ^7F_J low lying multiplet.[21]

Figure 2 compares the normalized excitation and emission spectra of Eu^{3+} ions incorporated in the interlayer of Mica-2 upon aqueous cation exchange at room temperature (sample called Eu-Mica-2) and Eu^{3+} absorbed in Mica-2 at 300°C (sample treated at 300°C for 0 days in Figure 1a). The narrow peaks observed in the excitation spectra (Figure 2a) correspond in both samples to f-f Eu^{3+} transitions from the $^7F_0$ ground state to different excited states. The most remarkable difference between both samples is the broad band observed below 300 nm, which can be assigned to either $O_2^- \rightarrow Eu^{3+}$ charge transfer or energy transfer from the host to Eu^{3+} ions. The intensity of this band is ca. one order of magnitude higher in the sample subjected to hydrothermal treatment. The bands observed in the emission spectra upon excitation at 393 nm (Figure 2b) are assigned in both samples to Eu^{3+} transitions from the $^5D_1$ and $^5D_0$ excited states to the ^7F_J low lying multiplets (see Figure 1b). It is worth pointing out that, while the red $^5D_0$ Eu^{3+} luminescence is common in many different hosts, the green Eu^{3+} emission from the $^5D_1$ is absent in the majority of the systems and it has never been observed before in other silicate-type phases including montmorillonite and saponite, except in these Eu^{3+}-doped high charge micas.

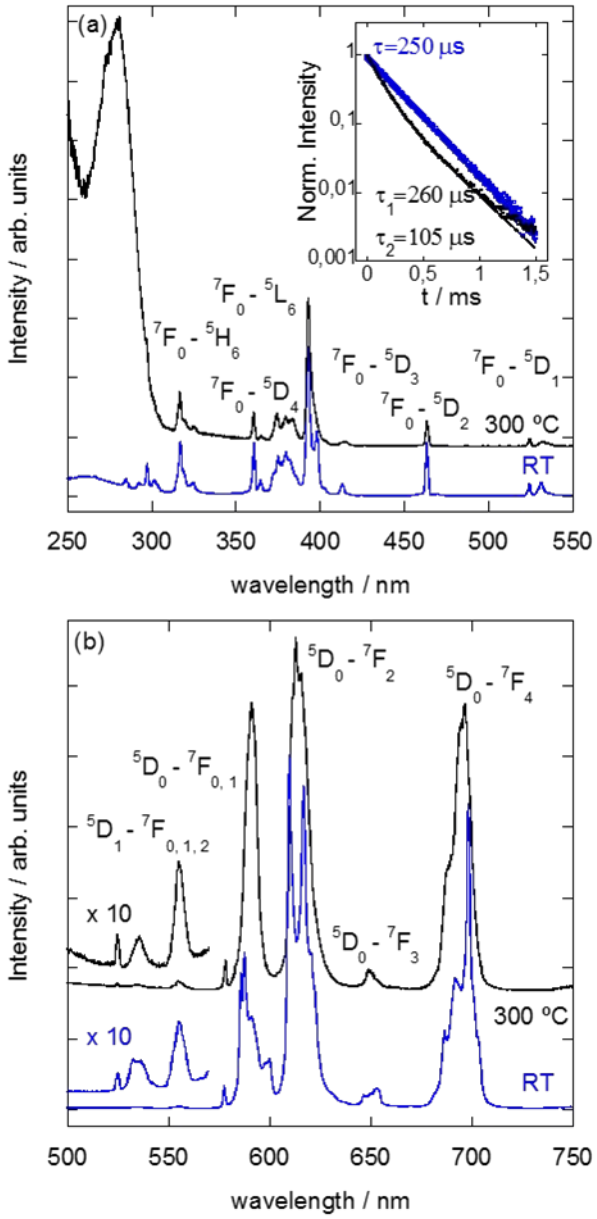

Figure 2. (a) Excitation spectra recording emission at 614 nm and (b) emission spectra upon excitation at 393 nm of Eu^{3+} in the sample Eu-Mica-2 (blue) and Mica-2 heated with a Eu^{3+} aqua-solution at 300°C (black). The inset shows the temporal evolution of the $^5D_0 \rightarrow {}^7F_J$ Eu^{3+} emission intensity, recorded at 614 nm upon excitation at 393 nm for both samples.

The emission features observed in Figure 2b have been recently associated to europium cations allocated in the interlayer space of the aluminosilicate.[21] Thus, the principal interaction mechanism for the sample heated at 300 °C, namely the incorporation of Eu^{3+} into the interlayer space of Mica-2, can be directly extrapolated from the luminescence measurements. Particularly, this mechanism is confirmed by the emission bands detected from both $^5D_1$ and $^5D_0$ excited states. However, the Eu^{3+} emission bands, especially the $^5D_0 \rightarrow {}^7F_1$ and $^5D_0 \rightarrow {}^7F_2$ transitions, show different crystal field components in the hydrothermally-treated sample and the Mica-2 exchanged at RT. Both transitions appear as broader bands in the sample treated at 300°C. Some disruption of the silicate network has been also proposed after the treatment,[23] and it is evidenced by the broadening of the $^5D_0 \rightarrow {}^7F_J$ transition bands in the emission spectra, and also the much broader band observed below 300 nm in the excitation spectra.

The temporal evolution of the $^5D_0 \rightarrow {}^7F_J$ Eu^{3+} luminescence intensity for both samples is also shown in the inset of Figure 2. The time dependence of the sample Eu-Mica-2 perfectly fits to a single exponential decay of 250 μs, evidencing the homogeneous distribution of Eu^{3+} ions in the interlayer of Mica-2. On the contrary, two different contributions, with 260 and 105 μs lifetimes, are observed in the sample after hydrothermal treatment at 300ºC. A lifetime of ca. 250 μs has been previously associated with Eu^{3+} cations situated in the hexagonal holes of the tetrahedral sheet in an inner-sphere conformation with 3 water molecules in the first coordination sphere.[21] Thus, the 260 μs lifetime can be ascribed to Eu^{3+} ions in the interlayer of the Mica-2 in a similar conformation, while the second contribution, with a lifetime of 105 μs, can be attributed to free Eu^{3+} aqua-ion adsorbed on the surface of the mica in outer-sphere complexation.[19] This extra Eu^{3+} is consistent with the slightly higher adsorption of europium cations during the treatment compared to its cation exchange capacity described in Figure 1.

3.3 Spectroscopic analysis of Eu^{3+} retention mechanisms in Mica-2

The photoluminescent properties of micas treated with a Eu^{3+} aqua-solution and subjected to different hydrothermal conditions have been investigated to analyze the potential of Eu^{3+} as an *in situ* optical sensor. The influence of both reaction temperature and time on the emission spectra and lifetime has been studied. In particular, the following Eu^{3+} luminescent features are highly interesting to be used as a sensor:[26] (1) the presence or absence of $^5D_1$ luminescence, which is extremely affected by non-radiative relaxation processes. (2) The position and width of the $^5D_0 \rightarrow {}^7F_0$ emission. This transition is strictly forbidden, shows the smallest line-width, and provides valuable information on the number of sites for Eu^{3+} ions. (3) The spectral shape of the $^5D_0 \rightarrow {}^7F_1$ emission, which is a magnetic dipole allowed transition. The presence of different crystal-field components in this transition indicates the existence of different crystalline sites. (4) The intensity ratio of the $^5D_0 \rightarrow {}^7F_1$ and $^5D_0 \rightarrow {}^7F_2$ emission peaks, which is usually used as a measure of the Eu^{3+} site inversion center. (5) The $^5D_0$ lifetime.

3.3.1 Influence of reaction temperature

Figure 3 presents the normalized excitation (a) and luminescence (b) spectra of the system Mica-2/Eu^{3+} solution, after hydrothermal treatment during 1 month and using different reaction temperatures, 150, 200 and 300°C. The excitation spectra were recorded detecting emission at 614 nm while luminescence spectra were obtained upon excitation at 393 nm. The excitation spectra consists of peaks which correspond to f-f Eu^{3+} transitions from the ground state to different excited states, as assigned in Figure 2a. Clearly, the peaks are narrower in the sample treated at 300°C. Besides, a rather broad band centered at 280 nm is observed only for the samples calcined at 150 and 200°C. This band has been previously assigned to the $O_2^- \rightarrow Eu^{3+}$

charge transfer in Mica-2 with Eu^{3+} cations localized in the interlayer space of the aluminosilicate.[21]

The emission peaks observed in the range 570-720 nm are assigned to the $^5D_0 \rightarrow {}^7F_J$ (J=0-4) Eu^{3+} transitions, while the less intense peaks (note the scale factor) detected in some cases below 570 nm are due to Eu^{3+} transitions from the $^5D_1$ excited state. Important differences are clearly observed in the emission spectra of different samples. Samples treated at 150 and 200°C show identical broader emission bands, which is consistent with slightly-distorted Eu^{3+}-doped Mica-2. On the contrary, the sample treated at 300°C presents sharper line emission, which can be attributed to a transition to new crystalline phases, in particular europium disilicate, $Eu_2Si_2O_7$, as well as europium aluminate, $EuAlO_3$, with different Eu^{3+} distribution within the host lattice, according to X-ray diffraction results, as it has been described elsewhere and introduced before (Figure 1).[23]

Firstly, Figure 3 clearly shows that Eu^{3+} green emission from the $^5D_1$ excited state is only observed for the samples treated at 150 and 200°C. $^5D_1$ luminescence is very sensitive to non-radiative relaxation processes caused by high phonon energy in the host material, cross-relaxation between Eu^{3+} ions or charge transfer processes. Cross-relaxation processes strongly depend on Eu^{3+} doping content, spatial distribution, and Eu^{3+}–Eu^{3+} interaction. The initial phase Mica-2 is completely exchanged with Eu^{3+}, which means that the Eu^{3+} content in the interlayer is the maximum allowed, and $^5D_1$ emission is always present in Mica-2. [21] Thus, the disappearance of this emission is necessarily due to a transformation to the silicate structure. Specifically, the samples calcined at 150 and 200ºC keep the layered structure of Mica-2, while the sample treated at 300°C has transformed into a different crystalline phases, mainly Eu_2SiO_4 and $Eu_2Si_2O_7$, where non-radiative de-excitation and cross-relaxation between Eu^{3+} ions is more competitive.

The absence of emission from higher energy levels ($^5D_1$) in those silicates can be attributed to either a multiphonon relaxation due to silicate group vibration (ca. 1000cm^{-1}),[27] or cross-relaxation between Eu^{3+} ions, since the minimum distance in this host matrix is 3.87 Å, shorter than the minimum Eu^{3+}-Eu^{3+} distance in Mica-2, 5.32 Å.[28]

Secondly, the observation of the $^5D_0 \rightarrow {}^7F_0$ transition in all samples indicates that Eu^{3+} ions occupy a C_{nv}, C_n or C_s symmetry site. More importantly, both the energy and the line width of this transition are highly sensitive to the local environment. The energy in gas phase is 17374 cm^{-1} and it is usually red-shifted as a consequence of the chemical bond, the shift being more remarkable for crystalline host materials.[26] In the samples treated at 150 and 200°C the $^5D_0 \rightarrow {}^7F_0$ transition is centered at ca. 17300 cm^{-1}, compatible with Eu^{3+} coordination with basal oxygens and water molecules, as in Mica-2. On the contrary, it appears shifted to 17275 cm^{-1} for the sample treated at 300°C, confirming the formation of more crystalline phases. Besides, there is also a clear difference in the line width, decreasing from 57 cm^{-1} to 21 cm^{-1}, for samples treated at 150 or 200°C and 300°C, respectively. This indicates that different environments are involved, as a result of differences in Eu^{3+}-ligand distances and angles, by comparison for instance with the bandwidth value of 2 cm^{-1} in Eu_2O_3.

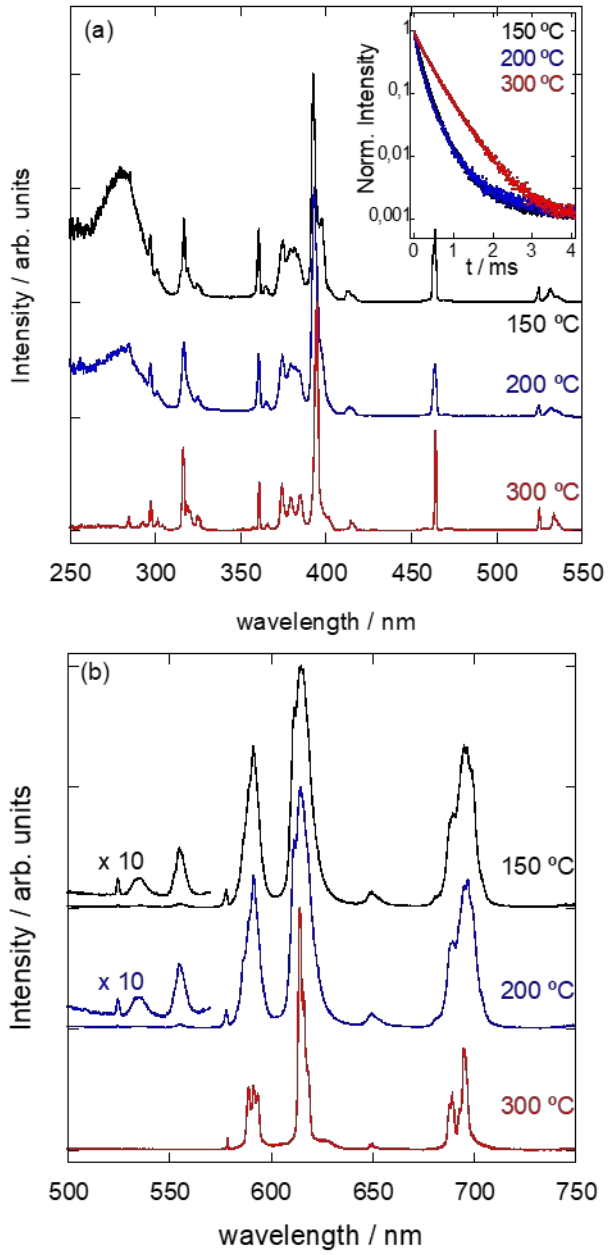

Figure 3. (a) Excitation spectra recording emission at 614 nm and (b) emission spectra upon excitation at 393 nm of the system Mica-2/Eu^{3+} aqueous solution, treated at 150, 200 and 300°C during 1 month. The inset shows the temporal evolution of the $^5D_0 \rightarrow {}^7F_J$ Eu^{3+} luminescence of Eu^{3+}-exchanged Mica-2 treated at 150, 200 and 300°C during 1 month, after excitation at 393 nm and recorded at 614 nm.

Thirdly, regarding the spectral shape of the $^5D_0 \rightarrow {}^7F_1$ emission, it is clear from Figure 3b that the samples treated at 150 and 200°C show a broader emission, while the sample heated at 300°C display three well-resolved peaks. This transition directly reflects the crystal-field splitting of the $^7F_1$ level. The fact that three sub-levels are observed for $^7F_1$ suggests that Eu^{3+} ions are in an orthorhombic or lower symmetry environment.[29,30,31] In addition, the intensity ratio of the $^5D_0 \rightarrow {}^7F_1$ and $^5D_0 \rightarrow {}^7F_2$ emission transitions displays also clear differences, being ca. 0.7 for the samples treated at 150 or 200°C, and 0.25 for the sample calcined at 300°C.

The inset in Figure 3 shows the temporal evolution of the $^5D_0 \rightarrow {}^7F_J$ Eu^{3+} emission intensity recorded upon excitation at 393 nm into the $^5L^6$ multiplet, for the Mica-2 after hydrothermal treatment with a Eu^{3+} aqueous-solution, during 1 month and different reaction temperatures, 150, 200 and 300°C. The experimental curves for the samples treated at 150 and 200°C present identical decay behavior, and have been fitted to a double exponential function, $I(t) = Ae^{-t/\tau_1} + Be^{-t/\tau_2}$. The two lifetimes obtained for both samples are τ_1=270 μs and τ_2=90 μs. τ_1 represents ca. 80% of total europium, and corresponds to Eu^{3+} ions located in the interlayer space, while τ_2 might be due to ions adsorbed on the mica surface. On the contrary, the decay curve of the sample heated at 300°C was fitted to a single exponential decay and shows a longer lifetime of 340 μs, evidencing the formation of new crystalline phases.

3.3.2 Influence of reaction time

Figure 4 shows the normalized excitation (a) and luminescence (b) spectra of Mica-2/$Eu(NO_3)_3$, after hydrothermal treatment at 300°C and different reaction times up to 1 month. The excitation spectra were recorded detecting emission at 614 nm while luminescence spectra were obtained

upon excitation at 393 nm. Considering the optical features described in the previous section, two distinguishable behaviors can be identified on the basis of the experimental excitation and emission spectra, the one detected for the initial sample and the observed for the samples treated for times longer than 2 days. Specifically, the sample treated at 0 days shows a broad excitation band below 300 nm, emission from the $^5D_1$ Eu^{3+} excited state, broader unresolved bands for the $^5D_0 \rightarrow {}^7F_J$ (J=0-4) transitions, and larger $^5D_0 \rightarrow {}^7F_1$ to $^5D_0 \rightarrow {}^7F_2$ intensity ratio. On the contrary, the spectral features are clearly distinct for longer treatment times. In particular, after 2-days treatment, both the broad excitation band at 280 nm and the emission from the $^5D_1$ Eu^{3+} excited state disappear. Besides, a shift of the $^5D_0 \rightarrow {}^7F_0$ emission to higher wavelength, a more structured $^5D_0 \rightarrow {}^7F_1$ transition, and a $^5D_0 \rightarrow {}^7F_1$ to $^5D_0 \rightarrow {}^7F_2$ intensity ratio smaller than 0.3 is observed. These luminescent features clearly evidence a mechanism of interlayer cation exchange for the system treated at 300°C 0 days, and a mechanism of chemical reaction for treatments longer than 2 days, in which silicon/aluminum atoms and Eu^{3+} interact to develop new crystalline phases, mainly disilicates, as well as ortosilicates and aluminates, to a lesser extent.

The inset in Figure 4 displays the time dependence of the $^5D_0 \rightarrow {}^7F_J$ Eu^{3+} emission intensity recorded upon excitation at 393 nm of the Eu^{3+} solution/Mica-2 system after hydrothermal treatment at 300°C and different reaction times. The observed decay curves were fitted to a double exponential curve, and the best fit parameters, τ_1 and τ_2, are shown in Table 1. Clearly, the lifetime values associated with structural Eu^{3+} ions, τ_1, gradually increase for longer treatments. Opposite to the excitation and emission spectral features which show abrupt changes above 2-day treatment, the experimental lifetime reveals a continuous character for the dependence of the phase transformation on the reaction time.

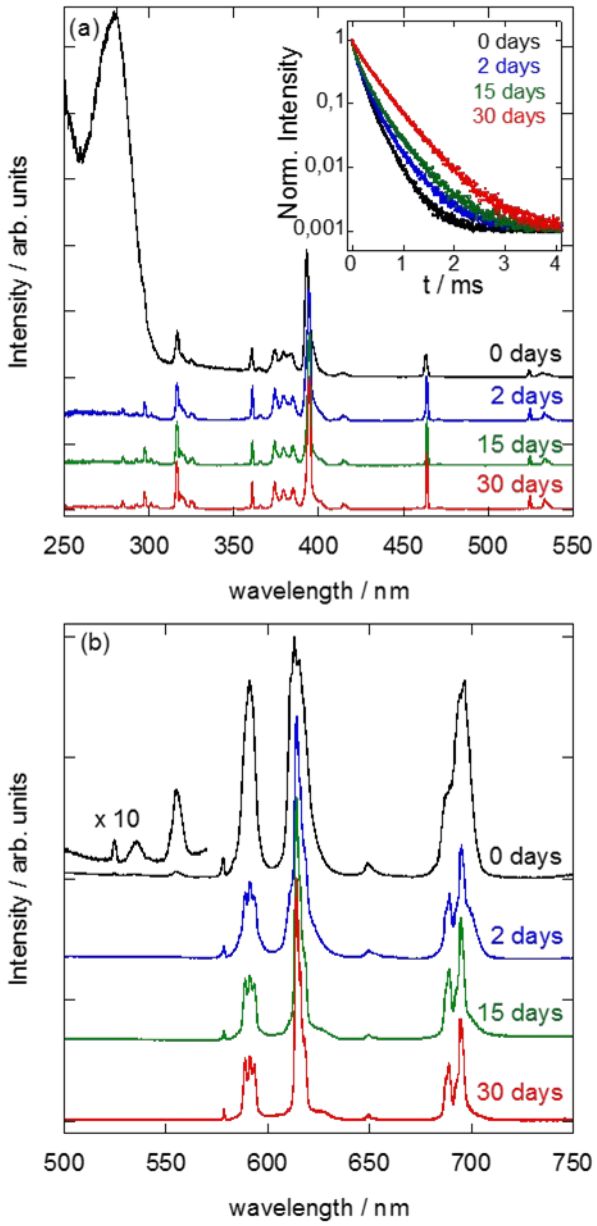

Figure 4. (a) Excitation spectra recording emission at 614 nm and (b) emission spectra upon excitation at 393 nm of Eu^{3+}-exchanged Mica-2 treated at 300°C during 0, 2, 15 and 30 days. The inset shows the time dependence of the $^5D_0 \rightarrow {}^7F_J$ Eu^{3+} luminescence recorded at 614 nm for all samples after excitation at 393 nm.

Table 1. Lifetimes of the $^5D_0$ Eu^{3+} excited state measured at 614 nm upon excitation at 393 nm, using a double exponential fitting, $I(t) = Ae^{-t/\tau_1} + Be^{-t/\tau_2}$.

Time / days	τ_1 / ms	τ_2 / ms
0	260	105
2	285	110
15	300	105
30	340	-

4. CONCLUSIONS

We have presented a new *in situ* optical sensor based on the incorporation of Eu^{3+} in Mica-2 for tracking the long-term physical-chemical behavior of HLW contaminants in DRG under mild hydrothermal conditions. Eu^{3+} acts not only as an actinide chemical analogue, but also, as an excellent luminescent probe to investigate the crystalline structure, since both the fine structure of different transitions and the emission lifetime can be used to characterize the local environment of Eu^{3+} cations. Besides, the innovative clay Mica-2, already proposed as an ideal candidate to be used in EBS, fulfils the purity and composition requirements to be used as a host for luminescent lanthanides. Two mechanisms are involved in the incorporation and subsequent immobilization of radioactive cations by the clay. The first process involved, an interlayer cation exchange, is characterized by the following Eu^{3+} luminescence features: green emission from the $^5D_1$ excited state, broader $^5D_0 \rightarrow {}^7F_0$ emission centered at higher energy, broader emission due to the $^5D_0 \rightarrow {}^7F_1$ transition, higher $^7F_1/^7F_2$ intensity ratio of ca. 0.7, and shorter luminescence lifetime. On the contrary, the second mechanism, the formation of new crystalline phases by the

interaction of the Si atoms of the aluminosilicate with the Eu^{3+} cations in the interlayer, is clearly identified by disappearance of the $^5D_1$ green emission, red-shift and narrowing of the $^5D_0 \rightarrow {}^7F_0$ transition, change in the spectral shape of the $^5D_0 \rightarrow {}^7F_1$ emission, lower $^7F_1/^7F_2$ intensity ratio and lengthening of the Eu^{3+} luminescence lifetime. Thus, Eu^{3+} luminescence in Mica-2 holds great potential as a new tool to analyze the process of HLW storage, from an initial reversible cation exchange reaction to the formation of new stable crystalline phases..

5. AUTHORS INFORMATION

Authors ORCID ID:

Rosa Martín-Rodríguez: 0000-0003-1568-5922

Fernando Aguado 0000-0003-2912-0228

María D. Alba 0000-0003-0025-3078

Rafael Valiente 0000-0001-9855-8309

Ana C. Perdigón 0000-0003-3865-3405

Corresponding Author

* QUIPRE department, University of Cantabria, Avda. De Los Castros 46, 39005, Santander, Spain.

Author Contributions

The manuscript was written through contributions of all authors.

6. ACKNOWLEDGMENT

Funding from projects MAT2015-63929-R, MAT2015-69508-P, PI16/00496 and NVAL16/17-IDIVAL is gratefully acknowledged.

7. ABBREVIATIONS

HLW, high-level radioactive waste; DGR, deep geological repositories; EBS, engineered barrier system.

8. REFERENCES

(1) General Safety Guide No. GSG-1: Classification of Radioactive Waste (IAEA, 2009).

(2) Carranza, M. R.; Rodríguez, M. A. Crevice Corrosion of Nickel-based Alloys Considered as Engineering Barriers of Geological Repositories. *Npj Materials Degradation,* **2017**, 1-9.

(3) Darley, H.C.H.; Gray, G.R. *Composition and Properties of Drilling and Completion Fluids* (Gulf Publishing Company, Houston, London, Paris, Zurich, Tokyo, 1988).

(4) Faybishenko, B.; Birkholzer, J.; Sassani, D.; Swift, P. (eds.) *International Approaches for Deep Geological Disposal of Nuclear Waste: Geological Challenges in Radioactive Waste Isolation: Fifth Worlwide Review* (Lawrence Berkeley National Laboratory, Sandia National Laboratories, 2016).

(5) Gregorkiewitz, M.; Raussell-Colom, J.A. Characterization and Properties of a New Synthetic Silicate with Highly Charged Mica-type Layers. *American Mineralogist,* **1987**, *72*, 515-527.

(6) Perdigón, A.C.; González, F.; Pesquera, C.; Li, D.; Blanco, C. Novel Acidic Solids from High Charge Na-micas by Mild Hydrothermal Treatment. *Micropor. Mesopor. Mater.,* **2010**, *133*, 100-105.

(7) Kodama, T.; Higuchi, T.; Shimizu, T.; Shimizu, K.; Komarneni, S.; Hoffbauer, W.; Schneider, H. Synthesis of Na-2-mica from Metakaolin and Its Cation Exchange Properties. *J. Mater. Chem.*, **2001**, *11*, 2072-2077.

(8) Trillo, J.M.; Alba, M.D.; Alvero, R.; Castro, M.A.; Muñoz-Paez, A.; Poyato, J. Interaction of Multivalent Cations with Layered Clays. Generation of Lutetium Disilicate upon Hydrothermal Treatment of Lu-Montmorillonite. *Inorg. Chem.*, **1994**, *33*, 3861-3862.

(9) Alba, M.D.; Castro, M.A.; Naranjo, M.; Pavón, E. Hydrothermal Reactivity of Na-n-Micas (n = 2, 3, 4). *Chem. Mater.*, **2006**, *18*, 2867-2872.

(10) Geckeis, H.; Lutzenkirchen, J.; Polly, R.; Rabung, T.; Schmidt, M. Mineral-Water Interface Reactions of Actinides. *Chem. Rev.*, **2013**, *113*, 1016-1062.

(11) Paulus, W.J.; Komarneni, S.; Roy, R. Bulk Synthesis and Selective Exchange of Strontium Ions in $Na_4Mg_6Al_4O_{20}F_4$ Mica. *Nature,* **1992**, *357*, 571-573.

(12) Komarneni, S.; Kozai, N.; Paulus, W.J. Superselective Clay for Radium Uptake. *Nature*, **2001**, *410*, 771.

(13) Allen, C.C.; Wood, M.I. Bentonite in Nuclear Waste Disposal: A Review of Research in Support of the Basalt Waste Isolation Project. *Applied Clay Science,* **1988**, *3*, 11-30.

(14) Yung, S.C.; Toyooka, R.T.; McCall, T.B. *Thermal analysis for BWIP waste package advanced conceptual design* (In:R Post, Waste Management 86. University of Arizona/American Nuclear Society, 1986).

(15) Alba, M.D.; Chain, P. Persistence of Lutetium Disilicate. *App. Geochem.,* **2005**, *22*, 192-201.

(16) Alba, M.D.; Becerro, A.I.; Castro, M.A.; Perdigón, A.C. Hydrothermal Reactivity of Lu-Saturated Smectites: Part I. A long-Range Order Study. *American Minealogist*, **2001**, *86*, 115-123.

(17) Bauer, A.; Rabung, T.; Claret, F.; Schäfer, T.; Buckau, G.; Fanghänel, T. Influence of Temperature on Sorption of Europium onto Smectite: The Role of Organic Contaminants. *Applied Clay Science*, **2005**, *30*, 1-10.

(18) Stumpf, T.; Bauer, A.; Coppin, F.; Kim, J. Inner-sphere, Outer-Sphere and Ternary Surface Complexes: a TRLFS Study of the Sorption Process of Eu(III) onto Smectite and Kaolinite. *Radiochimica Acta*, **2002**, *90*, 6, 345-349.

(19) Metz, E.; González-Robles, E.; Müller, N.; Bohnert, E.; Herm, M.; Lagos, M.; Kienzler, B.; Serrano-Purroy, D.; Fast/Instant Release of Safety Relevant Radionuclides from Spent Nuclear Fuel FIRST-Nuclides. Characterization of Spent Nuclear Fuel Samples and Description of Methodologies and Tools to be Applied in FIRST-NUCLIDES. Deliverable No 1.2. European Commission, Brussels (2013).

(20) Okada, T.; Ehara, Y.; Ogawa, M. Adsorption of Eu^{3+} to Smectites and Fluoro-Tetrasilicic Mica. *Clays and Clay Minerals*, **2007**, *55*, 4, 348-353.

(21) Martín-Rodríguez, R.; Valiente, R.; Aguado, F.; Perdigón, A.C. Highly Efficient Photoluminescence from Isolated Eu3+ Ions Embedded in High-Charge Mica. *J. Mater. Chem. C*, **2017**, *5*, 10360-10368.

(22) Silversmith, A. J.; Nguyen, T. T.; Campbell, D. L.; Boye, D. M.; Ortiz, C. P.; Hoffman, K. R. Fluorescence Yield in Rare-Earth-Doped Sol–Gel Silicate Glasses *J. Lumin*., **2009**, *129*, 1501-1504.

(23) García-Jiménez, M.J.; Cota, A.; Osuna, F.J.; Pavón, E.; Alba, M.D. Influence of Temperature and Time on the Eu^{3+} Reaction with Synthetic Na.-Mica-n (n = 2 and 4). *Chemical Engineering Journal*, **2016**, *284*, 1174-1183.

(24) Tertre, E.; Berger, G.; Simoni, E.; Castet, S.; Giffaut, E.; Loubet, M.; Catalette, H. Europium Retention onto Clay Minerals from 25 to 150 °C: Experimental Measurements, Spectroscopic Features and Sorption Modelling. *Geochim. Cosmocim. Acta,* **2006**, *70*, 4563-4578.

(25) Plancque, G.; Moulin, V.; Toulhoat, P.; Moulin, C. Europium Speciation by Time-Resolved Laser-Induced Fluorescence. *Anal. Chim. Acta*, **2003**, *478*, 11-22.

(26) Binnemans, K. Interpretation of Europium(III) Spectra. *Coord. Chem. Rev.* **2015**, *295*, 1-45.

(27) Deng, Y.; Song, W.; Dong, W.; Dai, R.; Wang, Z.; Zhang, Z.; Ding, Z. White Light Emission of Eu^{3+}/Ag Co-doped $Y_2Si_2O_7$. *Journal of Rare Earths,* **2014**, *32*, 9, 779-786.

(28) Felsche, J. The Crystal Chemistry of the Rare-Earth Silicates. Structure and Bonding (Berlin), 165 (1973).

(29) García, C.R.; Diaz-Torres, L.A.; Oliva, J.; Hirata, G.A. Green $EuAlO_3:Eu^{2+}$ Nanophosphor for Applications in WLEDs. *Optical Materials*, **2014**, *37*, 520-524.

(30) Busch, G.; Kaldis, E.; Verreault, R.; Felsche, J. A Phase Transition in Eu_2SiO_4. *Mat. Res. Bull.,* **1970**, *5*, 9-18.

(31) Fleet, M.E.; Liu, X. High-Pressure Rare Earth Disilicates $REE_2Si_2O_7$ (REE = Nd, Sm, Eu, Gd): Type K. *J. Solid State Chem.*, **2001**, *161*, 166-172.

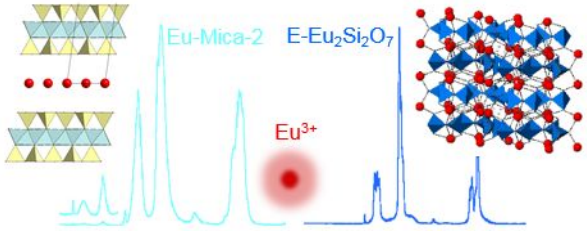

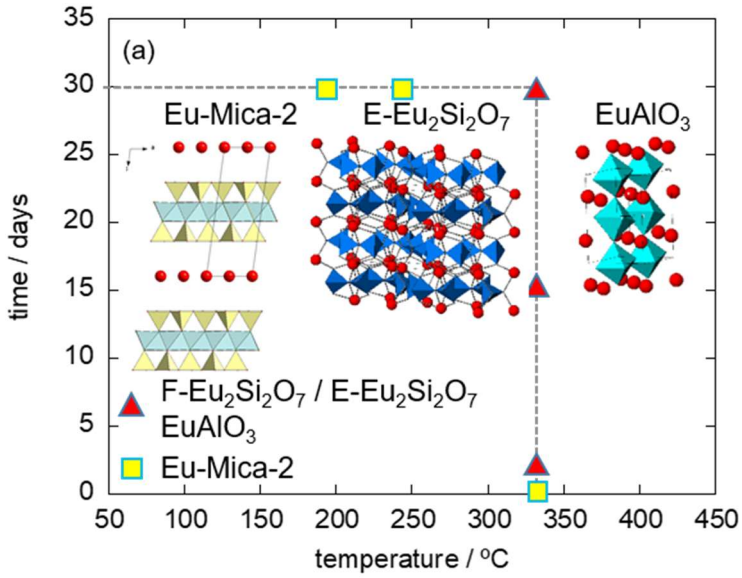
(a)
Eu-Mica-2
E-Eu2Si2O7
EuAlO3
time / days
temperature / °C
F-Eu2Si2O7 / E-Eu2Si2O7
EuAlO3
Eu-Mica-2

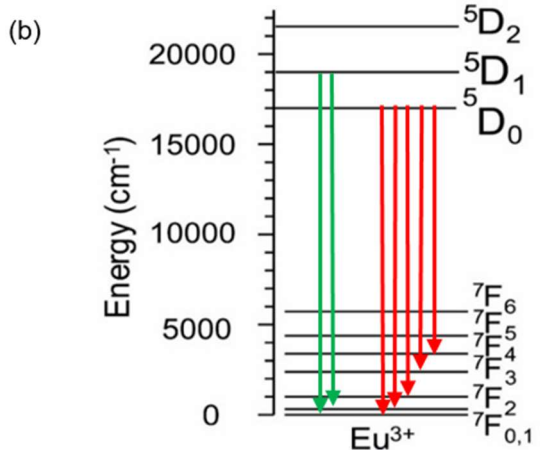
(b)
Energy (cm-1)
5D2
5D1
5D0
7F6
7F5
7F4
7F3
7F2
7F0,1
Eu3+

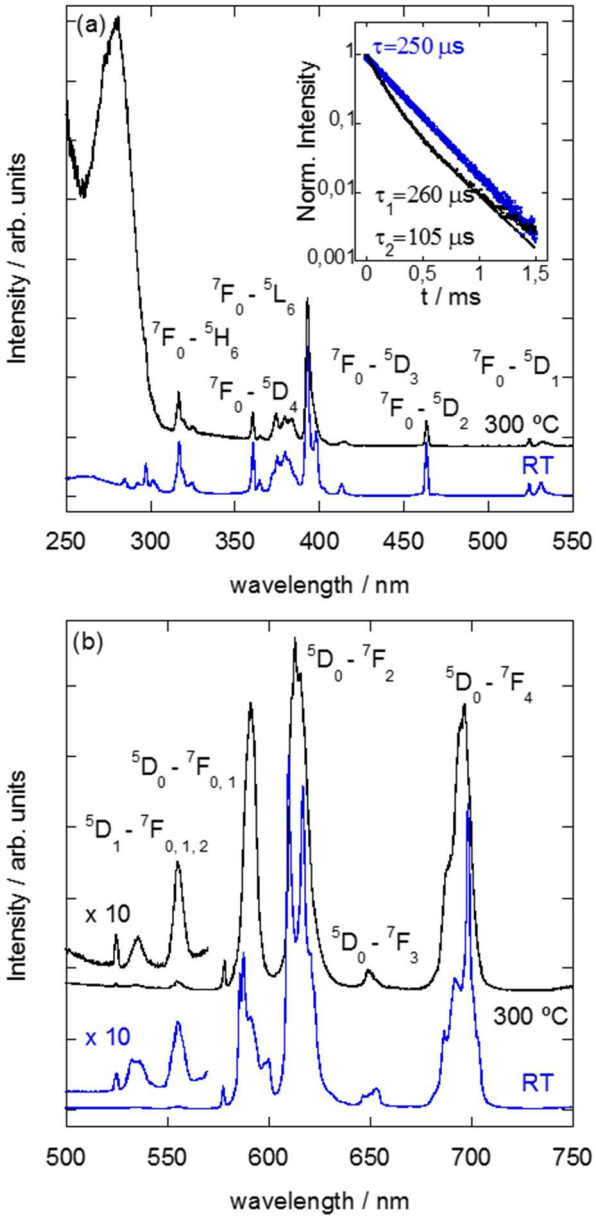
(a)
Intensity / arb. units
wavelength / nm
$^7F_0$ - $^5H_6$
$^7F_0$ - $^5L_6$
$^7F_0$ - $^5D_4$
$^7F_0$ - $^5D_3$
$^7F_0$ - $^5D_2$
$^7F_0$ - $^5D_1$
300 ºC
RT
τ=250 µs
Norm. Intensity
τ_1=260 µs
τ_2=105 µs
t / ms
(b)
$^5D_0$ - $^7F_{0,1}$
$^5D_1$ - $^7F_{0,1,2}$
$^5D_0$ - $^7F_2$
$^5D_0$ - $^7F_4$
$^5D_0$ - $^7F_3$
x 10
x 10
300 ºC
RT

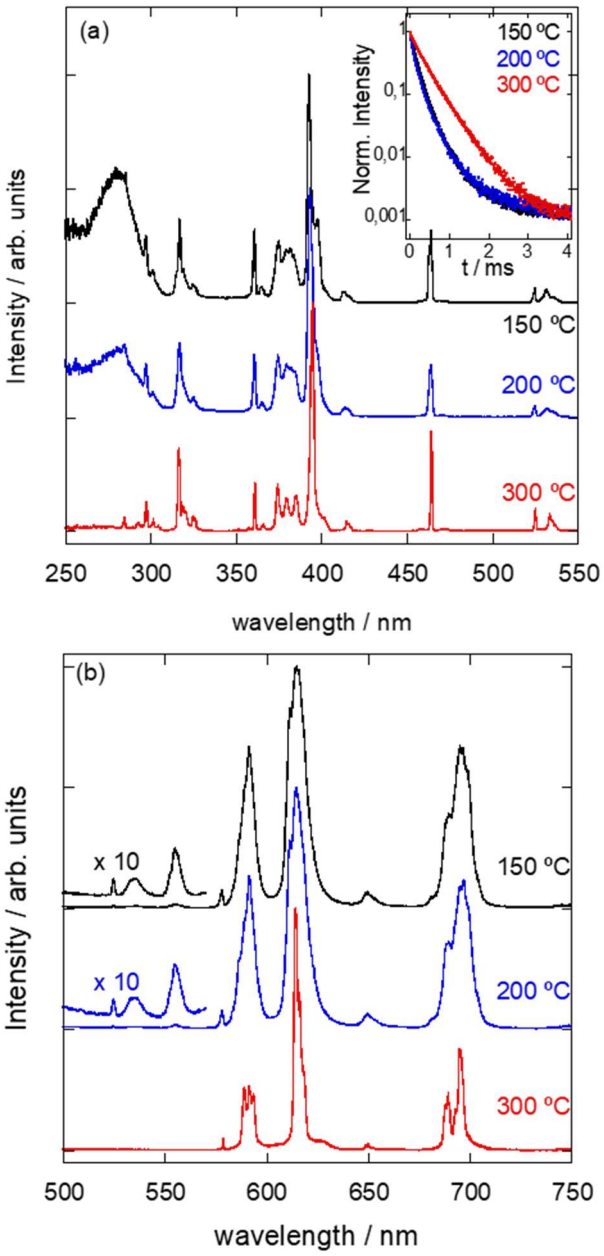
(a)
150 °C
200 °C
300 °C
Norm. Intensity
1
0,1
0,01
0,001
0
1
2
3
4
t / ms
Intensity / arb. units
250
300
350
400
450
500
550
wavelength / nm
(b)
x 10
x 10
150 °C
200 °C
300 °C
Intensity / arb. units
500
550
600
650
700
750
wavelength / nm

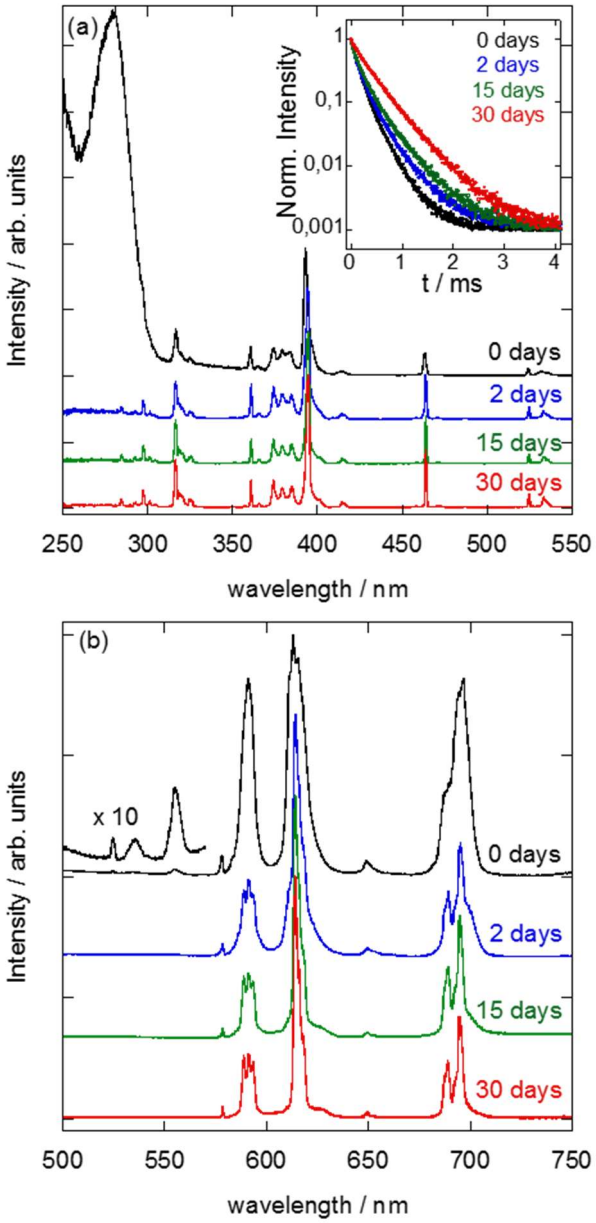
(a)
Intensity / arb. units
wavelength / nm
0 days
2 days
15 days
30 days
Norm. Intensity
t / ms
(b)
x 10
Intensity / arb. units
wavelength / nm
0 days
2 days
15 days
30 days